Journal of Materials Chemistry A

Accepted Manuscript

ROYAL SOCIETY OF CHEMISTRY

www.rsc.org/materialsA

Journal of Materials Chemistry A

ARTICLE

Achieving Ambient Temperature Hydrogen Storage in Ultrafine Nanocrystalline TiO_2@C-doped $NaAlH_4$

Received 00th January 20xx,
Accepted 00th January 20xx

DOI: 10.1039/x0xx00000x

www.rsc.org/

Yongfeng Liu,[a,b] Xin Zhang,[a] Ke Wang,[a] Yaxiong Yang,[a] Mingxia Gao[a] and Hongge Pan[a,*]

Sodium alanate ($NaAlH_4$) has attracted tremendous interest as a prototypical high-density complex hydride for on-board hydrogen storage. However, poor reversibility and slow kinetics limit its practical application. In this paper, we propose a novel strategy for the preparation of an ultrafine nanocrystalline TiO_2@C-doped $NaAlH_4$ system by first calcining the furfuryl alcohol-filled MIL-125(Ti) at 900 ºC and then ball milling with $NaAlH_4$ followed by a low-temperature activation process at 150 ºC under 100 bar H_2. The as-prepared $NaAlH_4$-9 wt% TiO_2@C sample releases hydrogen starting from 63 °C and re-absorbs starting from 31 °C, which are reduced by 114 °C and 69 °C relative to those of pristine $NaAlH_4$, respectively. At 140 °C, approximately 4.2 wt% of hydrogen is released within 10 min, representing the fastest dehydrogenation kinetics of any presently known $NaAlH_4$ system. More importantly, the dehydrogenated sample can be fully hydrogenated under 100 bar H_2 even at temperatures as low as 50 °C, thus achieving ambient-temperature hydrogen storage. The synergetic effect of the Al-Ti active species and carbon contributes to the significantly reduced operating temperatures and enhanced kinetics.

1. Introduction

One of the key enabling factors for using hydrogen as an energy carrier in a more sustainable future society is its storage in a safe, efficient, and reversible manner.[1] Compared to high pressure compression and liquefaction via cryogenics, solid-state hydrogen storage in metal hydrides has several attractive features, including high volumetric and gravimetric densities, good reversibility, low cost and unique safety.[2] Interstitial metal hydrides have exhibited excellent hydrogen storage reversibility under moderate pressure and temperature conditions.[3] However, limited hydrogen capacities (< 2 wt%) prevent them from usage in ever-expanding applications, especially in automotive applications.[4] In recent years, research has focused more and more on metal complex hydrides, many of which have more than 5.5 wt% gravimetric hydrogen storage capacities.[5-7] In particular, sodium alanate ($NaAlH_4$) has attracted intense interest as a prototypical high-density complex hydride, which is well known to release 7.5 wt% of hydrogen in three steps, as follows:[8]

$$NaAlH_4 \rightarrow \frac{1}{3}Na_3AlH_6 + \frac{2}{3}Al + H_2 \quad (3.7\ wt\%) \quad (1)$$

$$\frac{2}{3}Na_3AlH_6 \rightarrow 2NaH + \frac{2}{3}Al + H_2 \quad (1.9\ wt\%) \quad (2)$$

$$2NaH \rightarrow 2Na + H_2 \quad (1.9\ wt\%) \quad (3)$$

However, $NaAlH_4$ needs to be improved by the addition of catalysts and/or nanoconfinement in porous materials due to its poor reversibility and slow kinetics when used as a vehicular hydrogen storage material.[8-30]

Extensive research has shown that the introduction of catalysts is quite effective in reducing the operation temperature and improving the reversibility for hydrogen storage in $NaAlH_4$.[8-30] A wide variety of catalysts ranging from transition metals to rare earth metals to carbon-based materials have been investigated and developed experimentally.[8-29] Among them, Ti-containing materials are the most extensively studied catalysts so far.[8-18] In 1997, Bogdanović and Schwichardi first demonstrated that doping a few mol% of *β*-$TiCl_3$ and $Ti(OBu)_4$ significantly reduced the dehydrogenation temperature, enhanced the kinetics, and most importantly, improved the reversibility of hydrogen storage in $NaAlH_4$.[8] This result brought great progress towards practical applications. Subsequently, a large number of Ti compounds, such as $TiCl_3$, TiF_3, TiF_4, TiO_2, TiC, Ti_xAl_y, TiH_2, TiB_2, TiN, and MIL-125(Ti), have been examined for their performances in catalysis.[4-18] In particular, Lee et al. observed that the desorption kinetics and the reversibility of $NaAlH_4$ hydrogen storage catalysed by TiO_2 nanopowder were better than those of $TiCl_3$-catalysed $NaAlH_4$ hydrogen storage.[11] Suttisawat et al. reported that TiO_2 nanoparticles exhibited

[a] State Key Laboratory of Silicon Materials, Key Laboratory of Advanced Materials and Applications for Batteries of Zhejiang Province and School of Materials Science and Engineering, Zhejiang University, Hangzhou 310027, China, E-mail: hgpan@zju.edu.cn, Tel/Fax: +86-571-87952615
[b] Key Laboratory of Advanced Energy Materials Chemistry (Ministry of Education), Nankai University, Tianjin 300071, China

†Electronic Supplementary Information (ESI) available: Relative C and TiO_2 contents in TiO_2@C, comparison of hydrogen storage properties of catalysts-added $NaAlH_4$, comparison of the catalytic activities of as-prepared TiO_2@C with different FA infiltration times and different calcination temperatures, N_2 adsorption/desorption isotherms and pore size distribution of the as-prepared TiO_2@C, XRD and EDS results. See DOI: 10.1039/x0xx00000x Electronic Supplementary Information (ESI)

superior catalytic effects to those of Ti nanoparticles.[12] In particular, the onset dehydrogenation temperature of TiO_2-doped $NaAlH_4$ was further reduced from 155 to 140 °C during subsequent cycles.[12] The same phenomenon was also observed in MIL-125(Ti)-doped $NaAlH_4$.[18] In addition, other transition metals such as Sc, V, Zr, Fe, and Ni and Lanthanides (La, Ce, and Pr) were also proved experimentally to be good catalysts.[19-25] More attractively, co-dopants have exhibited much superior catalytic functions to using single dopants. It has been found that Ti and Zr could act in concert to optimise the dehydriding/rehydriding behaviour of $NaAlH_4$.[26,27] Wang and co-workers reported that the dehydrogenation rate of $NaAlH_4$ co-doped with Ti and Fe was 1.5 times that of Ti alone at 130 °C.[28] Recent investigations have expanded from bimetallic systems to carbon-based materials. For example, co-doping 2 mol% Ti and 10 wt% graphite obtained a three-fold increase in the hydrogen desorption kinetics in comparison with being doped with 2 mol% Ti alone.[29] A significantly increased available hydrogen capacity and improved cycling stability were observed for $NaAlH_4$ doped with a TiO_2/C composite due to the light weight of carbon, high catalytic activity on hydrogenation and good inhibition ability for particle growth and agglomeration of the active species.[27] Despite these intense research efforts, the operating temperatures for hydrogen storage in $NaAlH_4$ and the de-/hydrogenation kinetics still fall short of the requirements for practical applications. Therefore, it is of significant importance to further reduce the operating temperatures and to enhance the de-/hydrogenation kinetics of $NaAlH_4$.

In this work, we propose a novel strategy for the preparation of an ultrafine nanocrystalline TiO_2@C-doped $NaAlH_4$ system with extremely fast kinetics at low temperatures and high capacity retention. The ultrafine nanocrystalline TiO_2 nanoparticles with a mixed anatase/rutile structure supported on porous carbon (named TiO_2@C) were successfully synthesised by directly calcining the furfuryl alcohol-filled Ti-based metal-organic framework, MIL-125(Ti), at 900 °C. The ultrafine nanocrystalline TiO_2@C-doped $NaAlH_4$ system was then prepared by means of ball milling and a subsequent low-temperature activation process at 150 °C under 100 bar H_2. The as-prepared $NaAlH_4$-9wt% TiO_2@C sample released 4.1 wt% of hydrogen within 30 min at 120 °C, and full re-hydrogenation was achieved even at 50 °C and 100 bar H_2. More importantly, 98.9% of the hydrogen capacity was retained after 10 cycles. All of these performances are superior to those of any presently known $NaAlH_4$ system.

2. Experimental Section

2.1 Materials and Methods

All reagents and solvents were commercially available and used as received without further purification. MIL-125(Ti) was synthesised in our own laboratory following the procedure reported by Dan-Hardi et al.[33] Typically, titanium tetraisopropoxide ($Ti(OiPr)_4$, 2 mmol) and 1,4-benzene dicarboxylic acid (H_2BDC, 3 mmol) were added to a solution of dimethylformamide (DMF, 4.5 ml) and dry methanol (0.5 ml). The mixture was gently stirred at room temperature until the dicarboxylic acid had completely dissolved. The solution was transferred to an 80 ml Teflon liner, placed into a stainless steel autoclave, and heated at 150 °C for 15 h in a convection oven. After cooling to room temperature, the suspension was filtered, and the resulting precipitate was washed twice with DMF to remove the unreacted organic ligand and washed again with methanol to exchange the DMF with methanol. Finally, the solid-state product was activated under vacuum at 220 °C for 12 h.

After activation, MIL-125(Ti) (0.5 g), used as the hard framework, was mixed with a solution of furfuryl alcohol (FA, 30 ml) and ethanol (60 ml) with stirring (FA@MIL-125(Ti)). The whole mixture was stirred at room temperature under an Ar atmosphere for 24 h to ensure that the pores were filled with FA. After careful filtration and washing with ethanol to remove physically adsorbed FA on the surface, the FA@MIL-125(Ti) composite was transferred into a tube furnace under an Ar flow. The composite was first heated to 80 °C and dwelt for 24 h and then was further heated to 150 °C for 6 h to achieve the polymerisation of FA inside the pores of MIL-125(Ti). Afterward, the post-polymerised FA@MIL-125(Ti) was subjected to re-impregnation with FA followed by a secondary polymerisation process to obtain a high catalytic activity (Fig. S1, ESI †). Finally, the as-prepared PFA@MIL-125(Ti) (PFA: polymerised furfuryl alcohol) was calcined at 900 °C for 3 h to produce the resulting product composed of nanocrystalline TiO_2 and C (designated as TiO_2@C), which exhibited superior catalytic activity as shown in Fig. S2 (ESI †).

The $NaAlH_4$-x wt% TiO_2@C composites with x = 0, 1, 3, 5, 7, 9 and 10 were prepared by first ball milling the mixture of $NaAlH_4$ and TiO_2@C followed by a low-temperature heat treatment. Ball milling was conducted on a planetary ball mill (QM-3SP4, Nanjing) at 500 rpm for 24 h. The ball-to-sample weight ratio was approximately 120:1. To minimise the temperature increment of the samples during ball milling, the mill was set to rotate for 0.3 h in one direction, pause for 0.1 h, and then revolve in the reverse direction for 0.3 h. The as-milled samples were then transferred into a stainless-steel tube reactor for a low-temperature heat treatment under 100 bar hydrogen pressure at 150 °C for 2 h and then kept at 140 °C for another 1 h. All sample handling was conducted in a glove box (MBRAUN, Germany) filled with pure argon in which the H_2O and O_2 concentrations were kept below 1 ppm to prevent contamination from moisture and oxygen.

2.2 Property Evaluation

A home-built temperature-programmed desorption (TPD) system attached to an online gas chromatograph (GC) was used to qualitatively determine the temperature-dependent dehydrogenation behaviour. For each test, approximately 40 mg of the as-prepared sample was gradually heated from room temperature to 350 °C at 2 °C/min with pure argon as the carrier gas. Further quantitative evaluations of the dehydrogenation/hydrogenation reactions were conducted with a homemade Sieverts-type apparatus. Typically, 75 mg of

sample was loaded into a stainless steel tube reactor within a glove box, and the tube was then connected to the Sieverts-type apparatus. Both isothermal and non-isothermal modes were adopted. In the non-isothermal test, the temperature was gradually elevated from room temperature at a rate of 2 °C/min (starting from static vacuum) for dehydrogenation and 1 °C/min (with an initial hydrogen pressure of 100 bar) for hydrogenation. For the isothermal experiment, the sample was rapidly heated to the desired temperature, which was maintained during the entire test.

Pressure-composition isotherms (PCIs) for dehydrogenation were measured with a PCTpro-2000 (Hy-Energy, USA) operated up to temperatures of 140 – 170 °C. Before the measurements, the apparatus was carefully calibrated by helium gas. An ~ 0.5 g sample was tested. The sample holder had a thermocouple located in the centre of the sample to monitor the temperature in the reaction zone during dehydrogenation.

2.3 Structural and Morphological Characterisation

The phase structures of the samples were identified by powder X-ray diffraction (XRD). The XRD data were collected in a 2ϑ range of 10° – 90° with 0.05° step increments on an X'Pert Pro X-ray diffractometer (PANalytical, The Netherlands) with Cu Kα radiation at 40 kV and 40 mA. The powder samples were sealed in a specially designed container covered with Scotch tape to prevent air and moisture contamination. The constituent elements were analysed on a Vario MICRO cube elementary analyser (Elementer, Germany).

X-Ray photoelectron spectroscopy (XPS) examination was performed on a Kratos AXIS Ultra DLD spectrometer. The powder sample was compacted into a pellet at room temperature and mounted on the sample holder. The sample pellet was then transferred from the glove box into the XPS facility by a transfer vessel without exposing it to air. The XPS spectrum was recorded using a monochromatic Al Kα X-ray source with a base pressure of 6.8×10^{-9} Torr. The XPS data were calibrated using the adventitious C 1s signal at 284.6 eV as a reference, and the binding energy spectra were fitted by the XPSPEAK software.

The morphologies of the samples were observed using scanning electron microscopy (SEM, Hitachi, S-4800) and transmission electron microscopy (TEM, FEI, Tecnai G2 F20 S-TWIN). The distributions of elemental Na, Al, C, and Ti in the samples were detected with an energy-dispersive X-ray spectrometer (EDS) attached to a Hitachi S-3400 scanning electron microscope. Samples were quickly transferred from the glove box to the SEM facility under a nitrogen atmosphere to protect the powdery samples from contacting air during sample transfer. N_2 adsorption measurements were performed at 77 K, maintained by a liquid nitrogen bath, with relative pressures ranging from 0 to 1 bar using a NOVA-1000e automated surface area analyser (Quantachrome, USA).

3. Results and Discussion

3.1 Synthesis and Characterisation of Ultrafine Nanocrystalline TiO_2@C

Our synthesis of the ultrafine nanocrystalline TiO_2@C composite consists of a four-step process (Fig. 1a). The MIL-125(Ti) was first prepared by reacting titanium tetraisopropoxide ($Ti(OiPr)_4$) with 1,4-benzene dicarboxylic acid (H_2BDC) in a solution of dimethylformamide (DMF) and methanol. After 15 h of reaction in a sealed Teflon container at 150 °C, white powders were obtained, which were identified to be MIL-125(Ti) by X-ray diffraction (XRD) (Fig. S3, ESI †). Subsequently, the as-synthesised powders were immersed in ethanol solutions of FA and then filtered and washed with ethanol to produce the FA@MIL-125(Ti) composite. After that, brown powders of the PFA@MIL-125(Ti) (PFA: polymerised furfuryl alcohol) composite were formed by heating the FA@MIL-125(Ti) composite at 80 °C for 24 h and then at 150 °C for 6 h. Finally, black powders were obtained after calcining the PFA@MIL-125(Ti) composite at 900 °C. The resulting product was subject to powder X-ray diffraction examination (XRD) and scanning electron microscopy (SEM) and transmission electron microscopy (TEM) observations. As shown in Fig. 1b, the typical reflections of anatase and rutile TiO_2 were visible with considerable intensities in the XRD profile. This result indicates that the sample calcined at 900 °C was mainly composed of anatase and rutile TiO_2 as expected.[34] Energy-dispersive X-ray spectrometry (EDS) revealed that the resulting product was mainly composed of Ti, O, and C elements (Fig. S4, ESI †), and elemental analyses indicated that approximately 31 wt% C existed in the calcined product (Table S1 †). Further calculation gave a weight ratio of 1:0.98 for anatase and rutile TiO_2 according to the method proposed by Zhang et al.[35] Such a composite is expected to possess superior catalytic activity as observed previously in the TiO_2-catalysed H_2 production from water and methanol.[36]

Fig. 1(c-j) illustrates the SEM and TEM images of the as-calcined product at 900 °C. As shown in Fig. 1c, SEM observation shows that the sample mainly consists of polyhedral particles measuring < 1 μm in diameter. A closer examination of the SEM images in Fig. 1d reveals that there are a large number of bright small particles ranging from 10 to 20 nm in diameter inlaid on the surface of the irregular polyhedral matrix. On the basis of the EDS analysis (Fig. 1e and f) of a representative particle together with the XRD results (Fig. 1b), the bright spots were identified as small TiO_2 particles, and the grey matrix should be porous carbon material. We therefore conclude that the as-calcined product is composed of crystalline TiO_2 nanoparticles supported on porous carbon (denoted as nanocrystalline TiO_2@C), which is further evidenced by TEM observations. As shown in Fig. 1g and h, a large number of nanoparticles with sizes of < 10 nm are homogenously and finely dispersed in the porous carbon matrix. The high-resolution TEM (HRTEM) images in Fig. 1i and j display the anatase TiO_2 (1 1 2), (1 0 1), and (1 0 3) planes and the rutile TiO_2 (1 1 0), (2 1 0), (1 0 1), and (2 1 1) planes. The N_2 adsorption/desorption isotherms of the as-calcined product (Fig. S5a, ESI †) are typical I isotherms with a sharp uptake at

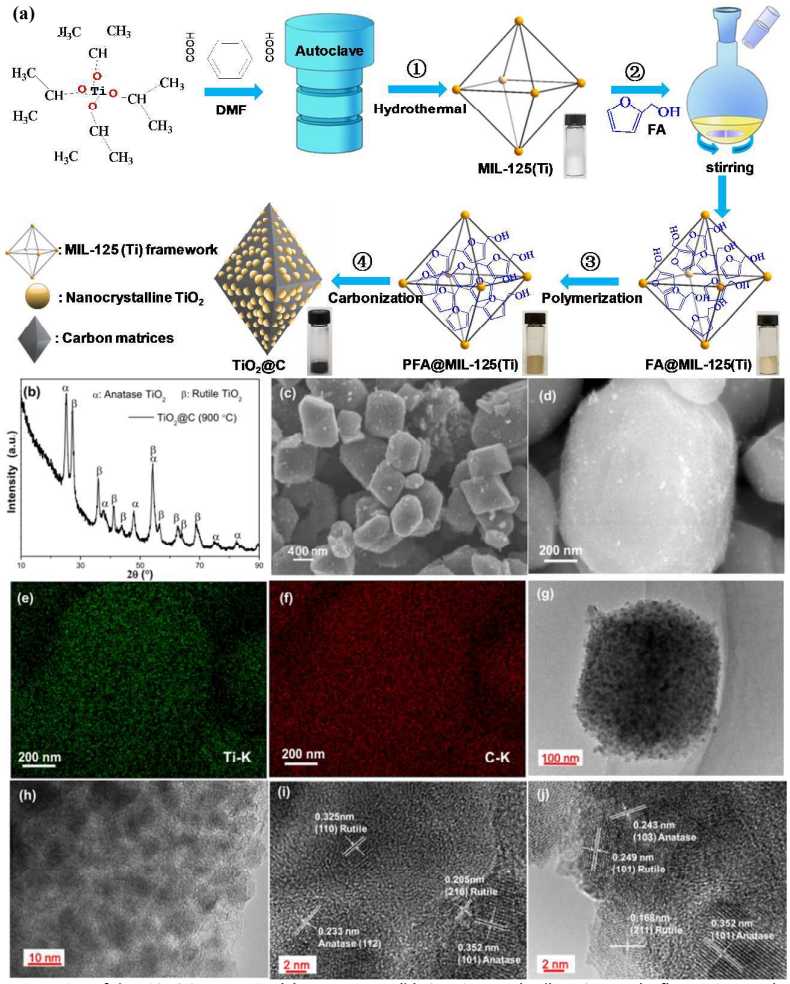

Fig. 1 Schematic illustration of the preparation of the TiO_2@C composite (a), XRD pattern (b), SEM images (c, d), EDS maps (e, f), TEM images (g, h), and HRTEM images (i, j) of the as-calcined TiO_2@C composite.

low relative pressures, suggesting that the pores in the carbon material are mostly micropores.[37] This is further confirmed by the measured pore size distribution (Fig. S5b, ESI †). The calculated micropore volume was 0.156 cm^3/g, and the total pore volume was 0.230 cm^3/g. As a consequence, the Brunauer-Emmett-Teller (BET) surface area was calculated to be 371 m^2/g. This small BET surface area suggests that most of the nanocrystalline TiO_2@C composite prepared in this case mainly consists of TiO_2 nanoparticles without a porous morphology, which make up most of the weight of the nanocomposite, as mentioned above (Table S1 †).

3.2 De-/Hydrogenation Properties of Ultrafine Nanocrystalline TiO_2@C-added $NaAlH_4$

The as-prepared nanocrystalline TiO_2@C composite was introduced into $NaAlH_4$ to evaluate the catalytic activity on the dehydrogenation/hydrogenation reaction. A series of composites with compositions of $NaAlH_4$-x wt% TiO_2@C (x = 0, 1, 3, 5, 7, 9, and 10) was prepared by first ball milling the mixture of $NaAlH_4$ and nanocrystalline TiO_2@C at 500 rpm for 24 h, then activated under 100 bar hydrogen pressure at 150 °C for 2 h, followed by keeping the sample at 140 °C for another 1 hour. The as-prepared TiO_2@C-added $NaAlH_4$ was collected for SEM observation and EDS analyses. As shown in Fig. S6a-b (ESI †), the ball milled sample mainly contained irregular particles measuring 500 nm to 2 µm in diameter, and Ti and carbon were homogenously dispersed on the surface of the $NaAlH_4$ particles. Fig. 2a presents a qualitative dehydrogenation behaviour of the as-prepared $NaAlH_4$-x wt% TiO_2@C composites measured by the temperature-programmed desorption (TPD) technique. As expected, the majority of the dehydrogenation of $NaAlH_4$ was significantly shifted toward lower temperatures after nanocrystalline TiO_2@C was added. The operating temperature of the maximum dehydrogenation peak was reduced from 260 °C for the pristine sample to 164 °C for the 1 wt% TiO_2@C-containing $NaAlH_4$, representing a 96 °C reduction. More encouragingly, by increasing the content of nanocrystalline TiO_2@C to 9 wt%, an additional 65 °C reduction was achieved because the majority of the dehydrogenation peak shifted to 99 °C. This temperature reduction is much superior to those obtained with the previously reported Ti-based additives (> 120 °C) (Table S2 †).[8-24] However, the last dehydrogenation peak was lowered by only 26 °C even though the content of

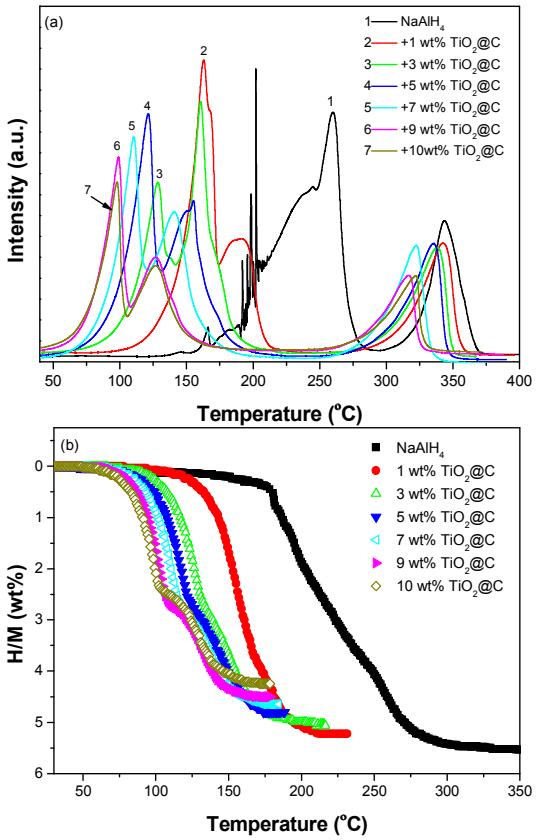

Fig. 2 TPD (a) and volumetric release (b) curves of $NaAlH_4$-x wt% TiO_2@C samples.

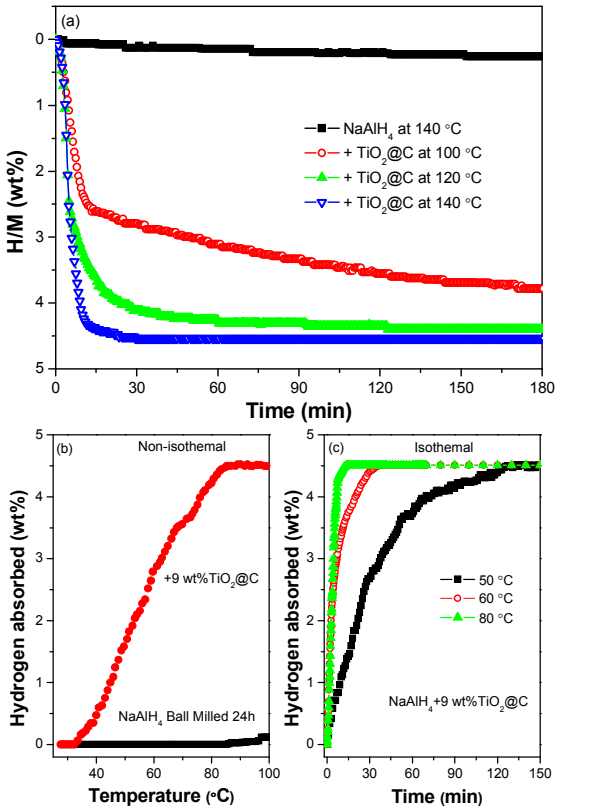

Fig. 3 De-/Hydrogenation curves of the $NaAlH_4$ with and without TiO_2@C: (a) isothermal dehydrogenation, (b) non-isothermal hydrogenation and (c) isothermal hydrogenation.

nanocrystalline TiO_2@C was 9 wt%. This result suggests that the nanocrystalline TiO_2@C additive is more effective in catalysing the decomposition of [AlH_4] and [AlH_6] than that of NaH. As a result, our follow-up quantitative evaluations of the dehydrogenation process are mainly concentrated on the first two steps.

Fig. 2b shows the volumetric release curves of the $NaAlH_4$-x wt% TiO_2@C composites. The volumetric release curves exhibit a distinctly compositional dependence of the nanocrystalline TiO_2@C-containing $NaAlH_4$. When 1 wt% TiO_2@C was added, the onset temperature for rapid dehydrogenation was reduced by 65 °C from 177 °C to 112 °C, and the terminal temperature for the second step of dehydrogenation was lowered by 96 °C from 308 °C to 212 °C. Adding more TiO_2@C further lowered the operating temperature for hydrogen release from $NaAlH_4$, i.e., hydrogen release from the sample with 9 wt% TiO_2@C began at only 63 °C and terminated at 170 °C, which are 49 °C and 42 °C lower than the corresponding temperatures for the sample with 1 wt% TiO_2@C, respectively. Thus, adding 9 wt% TiO_2@C into $NaAlH_4$ induces a significant reduction by 114 °C and 136 °C in the onset and terminal dehydrogenation temperatures, respectively. Additional reduction in the dehydrogenation temperature was not observed when the amount of TiO_2@C was further increased to 10 wt%. However, the dehydrogenation capacity of the samples continuously decreased from 5.5 wt% to 4.2 wt% because of the dead weight of the TiO_2@C additive. A careful comparison revealed that the $NaAlH_4$-9 wt% TiO_2@C composite possesses optimal dehydrogenation properties, i.e., it rapidly releases approximately 4.5 wt% of hydrogen at 65 °C – 175 °C in the non-isothermal mode.

Fig. 3a demonstrates the isothermal dehydrogenation curves of the pristine $NaAlH_4$ and $NaAlH_4$-9 wt% TiO_2@C samples. As shown in Fig. 3a, the $NaAlH_4$-9 wt% TiO_2@C sample rapidly released approximately 4.2 wt% of hydrogen within 10 min at 140 °C, corresponding to 93% of the available hydrogen capacity. However, no distinct hydrogen release was observed for the pristine $NaAlH_4$ at 140 °C. At 120 °C, the $NaAlH_4$-9wt% TiO_2@C sample released 4.1 wt% of hydrogen within 30 min. More importantly, even when operated at a temperature as low as 100 °C, the dehydrogenation amount of the $NaAlH_4$-9 wt% TiO_2@C sample reached 3.8 wt% within 180 min. Such dehydrogenation kinetics is quite superior to those of any presently known $NaAlH_4$ system (Table S2, ESI †).[8-32]

After full dehydrogenation at 140 °C, the products were subjected to hydrogenation under 100 bar hydrogen. Fig. 3b shows the non-isothermal hydrogenation curve of the dehydrogenated $NaAlH_4$-9 wt% TiO_2@C composite. For comparison, the hydrogenation behaviour of the dehydrogenated pristine sample under identical conditions is also shown in Fig. 3b. It is observed that the nanocrystalline TiO_2@C-containing sample began hydrogen uptake at only 31 °C, which is 54 °C lower than the corresponding temperature for the pristine sample. For comparison, a 59 °C reduction in

the starting hydrogenation temperature was previously reported in a TiO_2/C-containing system.[28-30] The reduction can potentially be attributed to the mixed anatase/rutile structure of TiO_2 obtained in the present study.[36] The hydrogen uptake amounted to 4.5 wt% when the sample was heated to 86 °C. However, no distinct hydrogen uptake was detected for the dehydrogenated pristine sample at the identical temperature. This result reveals that the hydrogenation properties of $NaAlH_4$ were significantly improved with the presence of nanocrystalline TiO_2@C.

Further isothermal hydrogenation measurements presented very rapid hydrogen uptake kinetics for the dehydrogenated TiO_2@C-containing sample. As shown in Fig. 3c, the full hydrogenation was achieved for the dehydrogenated TiO_2@C-containing sample even at the temperature as low as 50 °C, absorbing ~ 4.5 wt% of hydrogen within 130 min. To the best of our knowledge, the operating temperature of 50 °C is the lowest for hydrogenation of catalyst-doped $NaAlH_4$ reported to date (Table S2 †).[8-30] With increasing operating temperature, the hydrogenation rate sped up dramatically as expected. At 60 °C, full hydrogenation was completed within 40 min, and it took only 12 min to absorb 4.5 wt% of hydrogen at 80 °C. The superior hydrogenation kinetics can potentially be attributed to the synergetic effect of the Ti-based catalyst and carbon materials.[38-39] It is well known that the Ti active species on the surface of the Ti-doped $NaAlH_4$ facilitate the dissociation of H_2.[38] Moreover, the presence of carbon is also helpful for improving the hydrogenation kinetics as reported previously.[39] In the present study, the in-situ-synthesised nanocrystalline TiO_2@C composites are composed of both TiO_2 and microporous carbon, which deliver not only the Ti-based active catalyst but also carbon, consequently resulting in superior hydrogen storage kinetics. The positive effects of carbon on improving the hydrogen storage properties of $NaAlH_4$ were further confirmed by the fact that pure TiO_2, obtained by heating the TiO_2@C composite to 350 °C in air to burn out the carbon, exhibited relatively inferior effects in catalysing de-/hydrogenation of $NaAlH_4$ with respect to the TiO_2@C composite (Fig. S7, ESI †).

3.3 Dehydrogenation Kinetics and Thermodynamics of As-prepared Composites

The effects of the addition of nanocrystalline TiO_2@C on the dehydrogenation kinetics of $NaAlH_4$ were further evaluated quantitatively by measuring the activation energy (E_a) of the dehydrogenation reaction using Kissinger's method.[40] The results are presented in Fig. 4(a-b). The apparent activation energies (E_a) for the first and second steps of dehydrogenation of the 9 wt% TiO_2@C-containing sample were calculated to be 77.5 and 76.9 kJ/mol, respectively. These values are 34% and 36% lower than those of the pristine $NaAlH_4$ reported by Sandrock et al.[9] This decrease in activation energy is responsible for the significantly reduced operating temperatures for hydrogen storage in the TiO_2@C-containing samples.

Fig. 4c shows the pressure-composition-isotherm (PCI) curves for the dehydrogenation of the $NaAlH_4$-9 wt% TiO_2@C

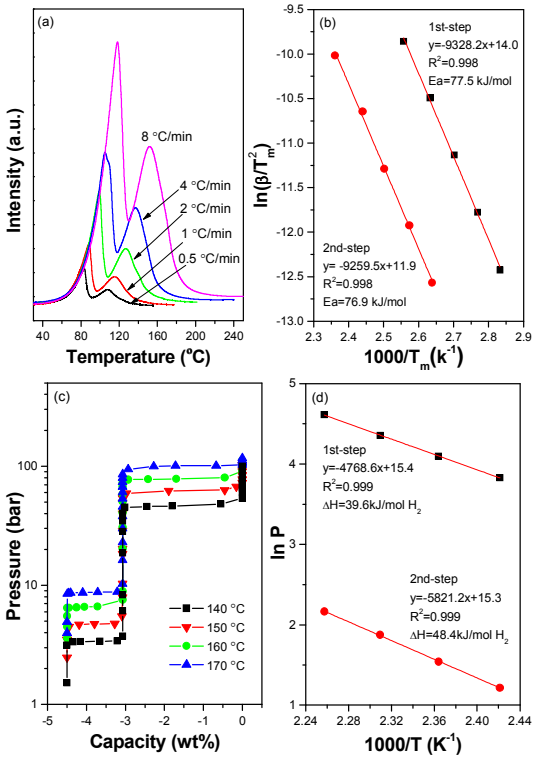

Fig. 4 TPD curves (a), Kissinger's plots (b), PCI curves (c) and van't Hoff plots (d) for the $NaAlH_4$-9 wt% TiO_2@C sample.

sample. Two distinct plateaus were observed in the PCI diagrams, corresponding to two steps of the dehydrogenation reaction of $NaAlH_4$. The higher plateau is attributed to the first dehydrogenation step described by reaction (1), and the lower plateau originates from the second dehydrogenation step described by reaction (2). By taking the middle of the plateaus, the desorption enthalpy change can be determined according to the van't Hoff equation.[10] As shown in Fig. 4d, the estimated enthalpy changes were 39.6 and 48.4 kJ/mol of H_2 for the first and second-step dehydrogenation, respectively, which are similar to those of the presently known Ti-doped $NaAlH_4$.[10] Extrapolating the fitting line shown in Fig. 4d to 1 bar equilibrium pressure results in dehydrogenation temperatures of 37 °C and 107 °C, which are in good agreement with the TPD and volumetric release results as shown in Fig. 2, thus achieving ambient temperature hydrogen storage in $NaAlH_4$.

3.4 Identifying Active Catalytic Species in the TiO_2@C-containing Samples

To understand the reason for the significantly reduced operating temperatures for hydrogen storage in the $NaAlH_4$-9 wt% TiO_2@C sample, the Ti states were characterised and analysed at various dehydrogenation stages. Fig. 5a and b show the XRD patterns of the as-prepared $NaAlH_4$-x wt% TiO_2@C (x = 0, 1, 3, 5, 7, 9, and 10) samples. It is seen that for all of the samples, the $NaAlH_4$ phase still dominated the XRD patterns with considerable intensities. With increasing addition of TiO_2@C, three new phases of Na_3AlH_6, Al and NaOH were also identified, although their intensities were rather low, suggesting that there was a chemical reaction between TiO_2 and $NaAlH_4$. A careful examination at the 2ϑ

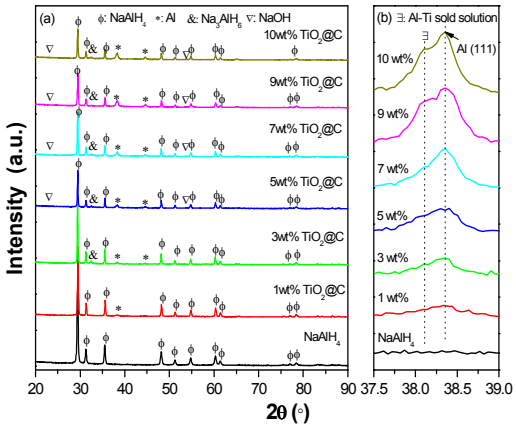

Fig. 5 XRD patterns of the as-prepared $NaAlH_4$-x wt% TiO_2@C samples.

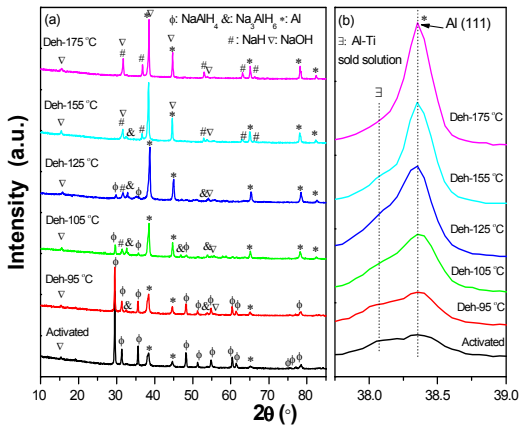

Fig. 6 (a) XRD patterns of dehydrogenated 9 wt% TiO_2@C-containing samples and (b) enlarged Al (111) peaks of TiO_2@C-containing samples at different stages.

range of 37.5 – 39.0° reveals that a shoulder appeared on the low-angle side of the Al (111) peak (2θ ~ 38.1°) and developed gradually into a new separate diffraction peak with increasing addition of the TiO_2@C composite (Fig. 5b). The slightly lower 2ϑ angle represents an enlarged lattice parameter relative to the pure Al, which is possibly because a small amount of Ti was dissolved into Al to form an Al-Ti solid solution phase because the atomic radius of Ti (2.0 Å) is larger than that of Al (1.82 Å). Such conjecture was further evidenced by XPS examination. As shown in Fig. S8 (ESI †), the Ti XPS spectrum displays a Ti $2p_{3/2}$ peak at 453.2 eV, which is very close to that of Al_3Ti (452.8 eV). It is therefore believed that the TiO_2 possibly reacted with $NaAlH_4$ to reduce Ti^{4+} to Ti^0 and that the newly developed metallic Ti was further dissolved into the lattice of Al to form an Al-Ti solid solution phase during ball milling and activation. More importantly, the Al-Ti solid solution phase formed in situ possesses much superior catalytic activity compared with the prepared TiO_2@C and TiF_3-added systems as shown in Fig. S9 (ESI †).

Fig. 6a and b show the XRD patterns of the dehydrogenated $NaAlH_4$-9 wt% TiO_2@C samples as a function of temperature. After dehydrogenation at 95 °C, the characteristic reflections of Na_3AlH_6 were detected with the intensification of the Al peaks, although $NaAlH_4$ was still the primary phase (Fig. 6a). When the dehydrogenation temperature was elevated to 105 °C, Na_3AlH_6 and Al dominated the XRD profile, and the $NaAlH_4$ peaks were dramatically weakened. At the same time, the strongest diffraction peak of NaH at 2ϑ = 36.7° emerged. By increasing the dehydrogenation temperature to 125 °C, the newly developed Na_3AlH_6 peaks weakened, and the $NaAlH_4$ phase was barely detectable. However, the diffraction peaks of NaH and Al were appreciably intensified and even became the dominant phases. Further elevating the temperature to 155 °C led to the near disappearance of Na_3AlH_6 along with further intensification of NaH and Al. While dehydrogenation stopped at 175 °C, the typical reflections of NaH and Al were distinctly intensified as the primary phases. In addition, it should be mentioned that NaOH was still observed throughout the dehydrogenation process. At the same time, a closer examination reveals that the shoulder on the low-angle side of the Al (111) peak persisted during dehydrogenation, although the relative intensity decreased with the intensification of the Al phase (Fig. 6b). This result indicates that the Al-Ti solid solution phase formed in the ball milling and activation process remains nearly constant during the following dehydrogenation. According to the above discussion, we conclude that the majority of hydrogen release from the nanocrystalline TiO_2@C-containing $NaAlH_4$ can still be described by reactions (1) and (2) as mentioned in the introduction, and the Al-Ti solid solution phase formed in situ plays a crucial role in catalysing hydrogen release from $NaAlH_4$.

3.5 Hydrogen Storage Cyclability of TiO_2@C-containing $NaAlH_4$

To evaluate the hydrogen storage cyclability of the nanocrystalline TiO_2@C-containing $NaAlH_4$, the sample was subjected to cycled dehydrogenation at 140 °C and hydrogenation at 100 °C under 100 bar hydrogen pressure. The results are shown in Fig. 7a. The nanocrystalline TiO_2@C-containing sample exhibited quite good cyclability. Its hydrogen desorption amounted to 4.5 wt% in the first cycle and remained at 4.46 wt% after 10 cycles. Thus, the capacity retention was calculated to be 98.9% (Fig. 7d), which is distinctly superior to that of any other Ti-doped $NaAlH_4$ (Table S2, ESI†).[11-21] Further non-isothermal experiments confirmed the nearly unchanged dehydrogenation/hydrogenation behaviours (Fig. 7b). For comparison, the cycling curves of the pristine sample were also measured for dehydrogenation at 250 °C and rehydrogenation at 220 °C. As shown in Fig. 7c, it was observed that only 2.1 wt% of hydrogen was reloaded at 220 °C under 100 bar hydrogen pressure, although the pristine $NaAlH_4$ released 5.5 wt% of hydrogen in the first cycle. After 5 cycles, the reversible hydrogen capacity stayed at 1.6 wt% under the testing conditions, representing a capacity retention of 29% (Fig. 7d). Hence, the addition of nanocrystalline TiO_2@C significantly improved the cycling stability of hydrogen storage in $NaAlH_4$. It is well known that upon cycling, the agglomeration of the hydrides and segregation of Al is responsible for the rapid degradation of the reversible hydrogen capacity of pristine $NaAlH_4$.[41] In the TiO_2@C-containing sample, however, EDS mapping revealed a very uniform distribution of Na, Al, Ti, and C elements after 10

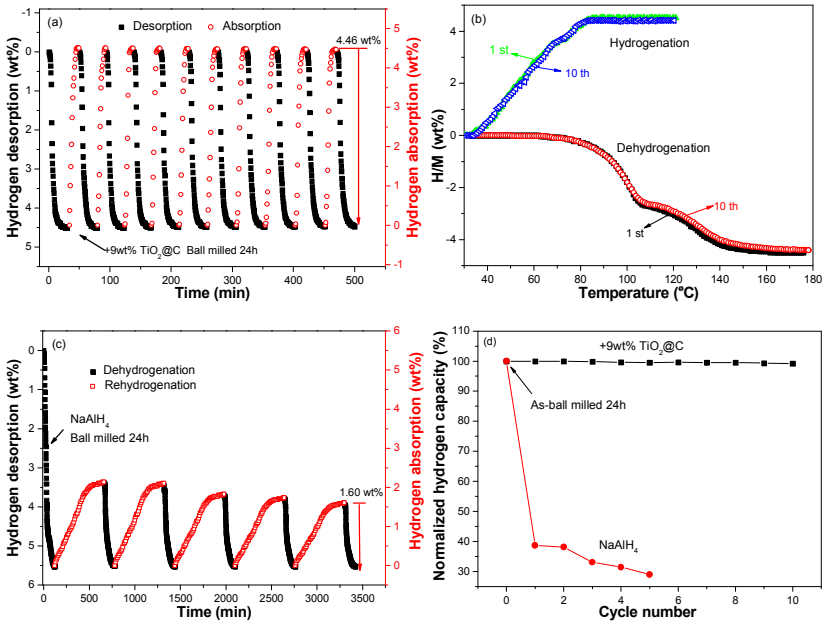

Fig. 7 (a) Reversible H_2 absorption (at 100°C under 100 bar H_2) and desorption (140°C) of the 9 wt% TiO_2@C-containing sample. (b) Non-isothermal dehydrogenation /hydrogenation curves (2 °C/min) of the 9 wt% TiO_2@C-containing sample at the 1st and 10th cycles (c) Reversible H_2 absorption (at 220°C under 100 bar H_2) and desorption (240 °C) of ball-milled $NaAlH_4$. (d) Cyclic capacity retention of $NaAlH_4$ with and without 9 wt% TiO_2@C.

cycles (Fig. S10, ESI †). This fact indicates that the phase segregation and agglomeration of NaH, Al and Ti-based active species were effectively prevented by adding the nanocrystalline TiO_2@C, and consequently, a high catalytic activity and good cycling stability were preserved. In addition, XRD analysis revealed that an Al-Ti solid solution phase was still detected during the cycling process (Fig. S11, ESI †), which is another important reason for the significantly improved cycling stability of the nanocrystalline TiO_2@C-containing $NaAlH_4$.

4. Conclusions

In this work, we have successfully synthesised a novel ultrafine nanocrystalline TiO_2@C-doped $NaAlH_4$ system by first calcining furfuryl alcohol-filled MIL-125(Ti) at 900 °C, then ball milling with $NaAlH_4$, followed by a low-temperature activation process at 150 °C under 100 bar H_2. The onset temperature of hydrogen desorption for the sample containing 9 wt% TiO_2@C was only 63 °C, which is 114 °C lower than that of pristine $NaAlH_4$. Moreover, it rapidly released approximately 4.2 wt% of hydrogen within 10 min at 140 °C, corresponding to 93% of the available hydrogen capacity. Even at 100 °C, the dehydrogenation amount of the $NaAlH_4$-9 wt% TiO_2@C sample reached 3.8 wt% within 180 min. The dehydrogenated TiO_2@C-containing sample was fully hydrogenated at 31 – 86 °C under 100 bar hydrogen pressure in the non-isothermal mode. More importantly, isothermal hydrogenation revealed that the full hydrogenation was achieved for the dehydrogenated TiO_2@C-containing sample at temperatures as low as 50 °C, absorbing approximately 4.5 wt% of hydrogen within 130 min, which is the lowest hydrogenation temperature for $NaAlH_4$ reported to date. The formation of an Al-Ti solid solution phase and the presence of porous carbon were believed to be the most important reasons for the reduced operating temperature and improved kinetics. In addition, the nanocrystalline TiO_2@C-containing sample exhibited quite good cyclability as the capacity retention was determined to be 98.9% after 10 cycles. The homogenous distribution of NaH, Al and Ti-based active species in the cycled sample is responsible for the significantly improved cycling stability of the nanocrystalline TiO_2@C-containing $NaAlH_4$.

Acknowledgements

We gratefully acknowledge the financial support received from the National Natural Science Foundation of China (51222101, 51171170), the Research Fund for the Doctoral Program of Higher Education of China (20130101110080, 20130101130007), the Zhejiang Provincial Natural Science Foundation of China (LR16E010002), and the Program for Innovative Research Team in University of Ministry of Education of China (IRT13037).

Notes and references

1 L. Schlapbach and A. Züttel, *Nature* 2001, **414**, 353.
2 K. J. Michel and V. Ozoliņš, *MRS Bull.*, 2013, **38**, 462.
3 J. Graetz and B. C. Hauback, *MRS Bull.*, 2013, **38**, 473.
4 G. Sandrock, *J. Alloys Compd.* 1999, **293-295**, 877.
5 S. Orimo, Y. Nakamori, J. R. Eliseo, A. Züttel and C. M. Jensen, *Chem. Rev.* 2007, **107**, 4111.
6 J. Yang and S. Hirano, *Adv. Mater.* 2009, **21**, 3023.
7 M. B. Ley, L. H. Jepsen, Y. S. Lee, Y. W. Cho, J. M. B. Von Colbe, M. Dorhi, M. Rokni, J. O. Jensen, M. Sloth, Y. Filinchuk, J. E. Jørgensen, F. Besenbacher and T. R. Jensen, *Materials Today* 2014, **122-128**, 17.

8 B. Bogdanović and M. Schwickardi, *J. Alloys Compd.* 1997, **253**, 1.
9 G. Sandrock, K. Gross and G. Thomas, *J. Alloys Compd.* 2002, **330-332**, 683.
10 B. Bogdanović, R. A. Brand, A. Marjanović, M. Schwickardi and J. Tölle, *J. Alloys Compd.* 2000, **302**, 36.
11 G. J. Lee, J. H. Shim, Y. W. Cho and K. S. Lee, *Int. J. Hydrogen Energy* 2008, **33**, 3748.
12 P. Rangsunvigit, Y. Suttisawat, B. Kitiyanan and S. Kulprathipanja, *Int. J. Energy Research* 2013, **37**, 713.
13 M. P. Pitt, P. E. Vullum, M. H. Sørby, M. P. Sulic, C. M. Jensen, J. C. Walmsley, R. Holmestad and B. C. Hauback, *Acta Mater.* 2008, **56**, 4691.
14 P. Wang, X. D. Kang and H. M. Cheng, *ChemPhysChem* 2005, **6**, 2488.
15 Y. F. Liu, F. H. Wang, Y. H. Cao, M. X. Gao, H. G. Pan, and Q. D. Wang, *Energy Environ. Sci.* 2010, **3**, 645.
16 L. Li, F. Y. Qiu, Y. P. Wang, Y. J. Wang, G. Liu, C. Yan, C. H. An, Y. A. Xu, D. W. Song, L. F. Jiao and H. T. Yuan, *J. Mater. Chem.* 2012, **22**, 3127.
17 J. W. Kim, J. H. Shim, S. C. Kim, A. Remhof, A. Brogschulte, O. Friedrichs, R. Gremaud, F. Pendolino, A. Züttel, Y. W. Cho and K. H. Oh, *J. Power Sources* 2009**, 192**, 582.
18 X. Zhang, Y. F. Liu, Y. P. Pang, M. X. Gao and H. G. Pan, *J. Mater. Chem. A* 2014, **2**, 1847.
19 Y. Song, J. H. Dai, C. G. Li and R. Yang, *J. Phys. Chem. C*, 2009, **113**, 10215.
20 B. Bogdanović, M. Felderhoff, A. Pommerin, F. Schüth, N. Spielkamp and A. Stark, *J. Alloys Compd.* 1997, **471**, 383.
21 M. Naik, S. Rather, R. Zacharia, C. S. So, S. W. Hwang, A. R. Kim and K. S. Nahm, *J. Alloys Compd.* 2009, **471**, L16.
22 T. Wang, J. Wang, A. D. Ebner and J. A. Ritter, *J. Alloys Compd.* 1997, **539**, 242.
23 J. J. Hu, S. H. Ren, R. Witter and M. Fichtner, *Adv. Energy Mater*. 2012, **2**, 560.
24 B. Bogdanović, M. Felderhoff, A. Pommerin, F. Schüth and N. Spielkamp, *Adv. Mater*. 2006, **18**, 1198.
25 T. Sun, B. Zhou, H. Wang and M. Zhu, *Int. J. Hydrogen Energy*, 2008, **33**, 2260.
26 R. A. Zidan, S. Takara, A. G. Hee and C. M. Jensen, *J. Alloys Compd.*, 1999, **285**, 119.
27 X. Z. Xiao, L. X. Chen, , X. H. Wang, S. Q. Li, C. P. Chen and Q. D. Wang, *Int. J. Hydrogen Energy*, 2008, **33**, 64.
28 J. Wang, A. D. Ebner, R. Zidan and J. A. Ritter, *J. Alloys Compd.*, 2005, **391**, 245.
29 J. Wang, A. D. Ebner, T. Prozorov, R. Zidan and J. A. Ritter, *J. Alloys Compd.*, 2005, **395**, 252.
30 R. J. Xiong, G. Sang, X. Y. Yan, G. H. Zhang, X. Q. Ye and X. L. Zhu, *Int. J. Hydrogen Energy*, 2011, **36**, 15652.
31 R. J. Xiong, G. Sang, X. Y. Yan, G. H. Zhang and X. Q. Ye, *J. Mater. Chem.*, 2012, **22**, 17183.
32 C. P. Baldé, B. P. C. Hereijgers, J. H. Bitter and K. P. Jong, *J. Am. Chem. Soc*. 2008, **130**, 6761.
33 M. Dan-Hardi, C. Serre, T. Frot, L. Rozes, G. Maurin, C. Sanchez and G. Ferey, *J. Am. Chem. Soc.* 2009, **131**, 10857.
34 X. B. Chen and S. S. Mao, *Chem. Rev.* 2007, **107**, 2891.
35 H. Z. Zhang, J. F. Banfield, *J. Phys. Chem. B* 2000, **104**, 3481.
36 J. Zhang, Q. Xu, Z. C. Feng, M. J. Li and C. Li, *Angew. Chem., Int. Ed.* 2008, **47**, 1766.
37 H. L. Jiang, B. Li, Y. Q. Lan, K. Kuratani, T. Akita, H. Shioyama, F. Q. Zong and Q. Xu, *J. Am. Chem. Soc.* 2011, **133**, 11854.
38 T. J. Frankcombe, *Chem. Rev.* 2012, **112**, 2164.
39 Y. W. Li, R. T. Yang, *J. Am. Chem. Soc.* 2006, **128**, 726.
40 H. E. Kissinger, *Anal. Chem.* 1957, **29**, 1702.
41 S. Y. Zheng, F. Fang, G. Y. Zhou, G. R. Chen, L. Z. Ouyang, M. Zhu and D. L. Sun, *Chem. Mater.* 2008, **20**, 3954.

Graphical contents entry

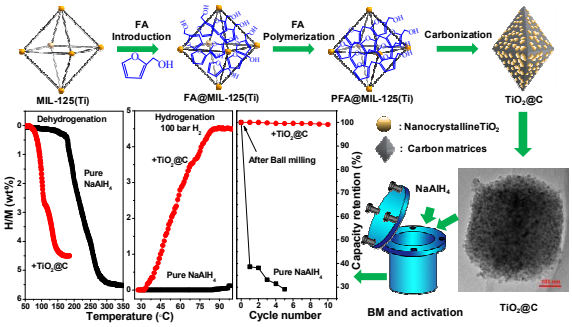

$NaAlH_4$ doped with 9 wt% nanocrystalline TiO_2@C achieves ambient temperature hydrogen storage.